Spatially Variant Resolution Modelling Using Redistributed Lines-of-Response and the Image Space Reconstruction Algorithm

Matthew G. Bickell, John Gillam, Roger Fulton, Johan Nuyts

***Abstract*—A spatially variant resolution modelling technique is presented which models the physical processes of the measurement during the iterative reconstruction. This is achieved by redistributing the line-of-response endpoints according to derived probability density functions describing the detector response function and photon acollinearity. When applying this technique it is shown that, to avoid mathematical inconsistencies and reconstruction artefacts, MLEM cannot be used for the reconstruction. The ISRA algorithm, after being adapted to a list-mode based implementation, is used instead since its structure is well-suited to this application. The Redistribution technique is shown to produce superior resolution recovery in off-centre phantom reconstructions than the standard stationary image-space Gaussian convolution approach, and it only requires approximately 35% more computation time.**

I. Introduction

In positron emission tomography (PET) imaging accurately modelling the physical measurement process to account for the point spread function (PSF) can improve the subsequent resolution of the reconstruction [1]. During iterative reconstruction the modelling of the PSF may be accomplished by convolving the image with a suitable Gaussian distribution before forward projection and after backprojection, as is a standard approach in maximum likelihood expectation-maximisation (MLEM) [2]. This Gaussian distribution is generally spatially invariant.

To model the true resolution more accurately a spatially variant model should be used. Using such a spatially variant model becomes significant when the object being scanned extends over a considerable portion of the scanner field-of-view (FOV) (as is often the case in human torso imaging), or when the object is allowed to move during the scan and thus has a different resolution response throughout the scan, such as in motion correction studies using animals or humans. A previously reported technique, referred to as the Redistribution technique [3] has been further developed and these developments are reported upon here. In this model the two most dominant factors affecting the PSF, namely the detector response function and the acollinearity of the photon pair, are modelled for the Siemens microPET Focus220 small animal scanner.

M. G. Bickell and J. Nuyts are with the Medical Imaging Research Center, Department of Nuclear Medicine, KULeuven, Belgium.

J. Gillam and R. Fulton are with the Brain & Mind Research Institute and the Faculty of Health Sciences, University of Sydney, Australia.

This work has been funded by the IMIR project of KULeuven and the MIRIAD SBO project of the IWT.

Similar techniques have been employed before in various ways to model the system matrix [4]–[10]. Moehrs *et al* [4] used multiple integrations of each LOR to determine the entire system matrix and use it within a sinogram-based MLEM reconstruction; Chen *et al* [5] used a multi-ray approach based on Monte Carlo techniques to construct a sensitivity image, and used this sensitivity image during simulated data reconstructions; Gillam *et al* [9] use a multi-ray technique to model the system matrix during MLEM reconstruction for an axial PET system, however they report that, to observe an improvement in resolution recovery, the method can be computationally expensive.

The approach which is presented in the current work models the system matrix on-the-fly without the need to perform a lengthy pre-calculation or storage of the system matrix, it requires only a single pass through the list-mode data per iteration, takes only approximately 35% more computation time than standard resolution modelling techniques, and produces a significantly enhanced resolution recovery for off-centre phantoms. It is shown that, for this approach, the MLEM algorithm may produce artefacts due to mathematical inconsistencies introduced when using a list-mode based implementation. Therefore the use of the image space reconstruction algorithm (ISRA) [11] is recommended and shown to not produce these artefacts.

II. Theory

For a particular detector pair, the probability density functions (PDFs) describing each detector's response to an incoming photon can be derived. These PDFs can be modified to also account for photon acollinearity. The suitable combination of these PDFs in the space between the detectors yields the tube-of-response (TOR) for that pair, which represents the row of the system matrix corresponding to that detector pair. By considering a measured line-of-response (LOR) between these detectors, one can assign the positions of their endpoints (i.e. "redistribute" the LOR) according to these PDFs, thus forming a single sample from the TOR. By repeatedly redistributing a particular LOR, the TOR is sampled many times and can thus be approximated. These redistributed LORs can then be used in an iterative list-mode reconstruction algorithm.

The system matrix can be denoted by a_{ij}, where i is the detector pair index (or, equivalently, the LOR index) and j is the image voxel index. Let Ψ^i denote the infinite set of all possible redistributions of LOR i, and let $\psi \in \Psi^i$. Then the

system matrix elements can be written as

$$a_{ij} = \sum_{r}^{\infty} g^{i}_{\psi_r j} \simeq \sum_{r}^{R} g^{i}_{\psi_r j}, \tag{1}$$

where $g^{i}_{\psi_r j}$ is the contribution of the redistributed LOR ψ_r to the voxel j and includes geometric factors as well as crystal efficiencies. This infinite summation can be truncated to R terms to be computationally feasible. Usually, ψ_r are sampled randomly from the set of Ψ^i. The TOR corresponding to LOR i is thus approximated, with the quality of the approximation increasing with increasing R.

A. List-mode MLEM with the Redistribution technique

The standard MLEM formulation, when applied to list-mode data [12], [13], is

$$\lambda_j^{n+1} = \frac{\lambda_j^n}{\sum_i^I a_{ij}} \sum_m^M a_{i_m j} \frac{1}{\sum_k^J a_{i_m k} \lambda_k^n} \tag{2}$$

$$= \frac{\lambda_j^n}{\sum_i^I a_{ij}} \sum_i^I \sum_\ell^{y_i} a_{ij} \frac{1}{\sum_k^J a_{ik} \lambda_k^n}, \tag{3}$$

where λ_j^n is voxel j of the current reconstruction at iteration n, J is the number of voxels in the image, M is the number of measured list-mode events, the index i_m is the LOR associated with list-mode event m, I is the total number of possible LORs, and y_i is the number of times that LOR i appears in the list-mode data. Subsets can be utilised when implementing this algorithm, in which case it is referred to as the ordered-subsets expectation-maximisation (OSEM) algorithm [14]. When we incorporate the redistribution model, (1), into (3), we arrive at

$$\lambda_j^{n+1} = \frac{\lambda_j^n}{\sum_i^I \sum_r^R g^i_{\psi_r j}} \left(\sum_i^I \sum_\ell^{y_i} \sum_r^R g^i_{\psi'_r j} \frac{1}{\sum_k^J \sum_r^R g^i_{\psi''_r k} \lambda_k^n} \right), \tag{4}$$

where ψ'_r and ψ''_r are different for every ℓ. Since each LOR usually appears many times within the list-mode stream, i.e. $y_i > 1$, it is tempting to set $R = 1$ and rely on the repetitions of each LOR to sample the TOR sufficiently,

$$\lambda_j^{n+1} = \frac{\lambda_j^n}{\sum_i^I \sum_r^R g^i_{\psi_r j}} \left(\sum_i^I \sum_\ell^{y_i} g^i_{\psi'_\ell j} \frac{1}{\sum_k^J g^i_{\psi''_\ell k} \lambda_k^n} \right). \tag{5}$$

This ensures that the implementation is computationally feasible since each list-mode event is only redistributed once per iteration. However, it is immediately obvious that, with the summation over multiple instances of $g^i_{\psi''_\ell k}$ now occurring in the numerator, the system matrix element a_{ik} is no longer approximated as defined by (1). This introduces artefacts into the reconstruction, particularly in low count regions and near the edge of the radioactive object, examples of which can be seen in figure 1(a). This problem can be solved by making R large, but this then increases the number of computations proportionally and makes the reconstruction take an unreasonable amount of time to complete. Part of the aim of this work was to develop a technique that does not take significantly more time than a standard MLEM reconstruction with resolution modelling.

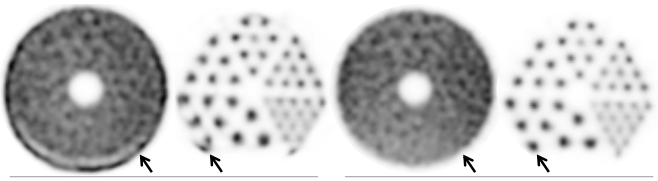

(a) (b)

Fig. 1. Showing two planes from (a) an MLEM reconstruction and (b) an ISRA reconstruction, both using the Redistribution technique with $R = 1$. In the MLEM reconstruction artefacts can be observed along the edge of the phantom, while the ISRA reconstruction is artefact free.

B. List-mode ISRA with the Redistribution technique

It was found that the structure of the Image Space Reconstruction Algorithm (ISRA) [11] was well suited to be used with this Redistribution technique since the forward and backprojection of the LORs both occur in the denominator. ISRA has the following sinogram-based formulation:

$$\lambda_j^{n+1} = \lambda_j^n \frac{\sum_i^I a'_{ij} q_i}{\sum_i^I a'_{ij} \sum_k^J a_{ik} \lambda_k^n}, \tag{6}$$

where q is the measured sinogram. If the system matrix used for the backprojection is the same as that used for the forward projection, i.e. $a'_{ij} = a_{ij}$, then the algorithm is a non-negative unweighted least squares algorithm [15]. In the original implementation of ISRA by Daube-Witherspoon *et al* a weighted least squares version was used since the normalisation factors were not used during the backprojection [11]. In [16] Reader *et al* discuss a generalised weighted least squares version of ISRA.

The formulation in (6) was adapted to be list-mode based. This was achieved by forward and backprojecting along all possible LORs in the denominator, which is equivalent to the sinogram-based approach except that no LORs were combined through mashing and spanning, as is done when binning LORs to a sinogram. The list-mode formulation can be written as

$$\lambda_j^{n+1} = \lambda_j^n \frac{\sum_m^M a_{i_m j}}{\sum_i^I a_{ij} \sum_k^J a_{ik} \lambda_k^n}, \tag{7}$$

using the same definitions as in (2). In practice the set of all possible LORs can be reduced to only those LORs passing through a volume enclosing the object (which will also be the reconstructed image space), which can provide a significant reduction in the number of LORs to be projected in comparison to a sinogram-based approach. During simulations it was found that the reconstructions using the Redistribution technique were very noisy due to the random redistribution of the LORs. To reduce this noise a combination of the Gaussian convolution technique and the Redistribution technique was

employed: the LORs were redistributed during the forward projection, but not during the backprojection, after which the backprojected image was convolved with a Gaussian distribution. As already indicated in (6), the forward and backprojections need not be exactly the same. It is only necessary that the two backprojections match and that the forward projection approximates the measurement process, which is satisfied by the Redistribution technique. This approach successfully reduces the noise while preserving the spatially variant nature of the model, and can be formulated by incorporating (1) into (7):

$$\lambda_j^{n+1} = \lambda_j^n \frac{\sum_{\xi}^{\Xi} G_{j\xi} \sum_{m}^{M} a_{i_m \xi}}{\sum_{\xi}^{\Xi} G_{j\xi} \sum_{i}^{I} a_{i\xi} \sum_{k}^{J} \sum_{r}^{R} g_{\psi_r k}^{i,n} \lambda_k^n} , \qquad (8)$$

where G is a Gaussian convolution kernel containing Ξ elements per voxel. As for the MLEM implementation, R is usually chosen to be 1. By increasing R the sampling of the PDFs is improved at the cost of computation time, but using $R = 1$ has proved to be sufficient. Improved sampling of the PDFs is instead achieved by performing a new redistribution of the LORs at the start of each iteration, as denoted by the index n in $g_{\psi_r k}^{i,n}$. This algorithm does not suffer from the artefacts that the MLEM formulation does, as can be seen in figure 1(b).

III. Experiments

The Siemens microPET Focus220 small animal scanner was used for our experiments. This scanner has an internal diameter of 258 mm, and a spatial resolution of 1.3 mm at the centre of the FOV. At a radial distance of 60 mm the spatial resolution degrades to $[1.9, 2.1, 3.2]$ mm in the tangential, axial, and radial components respectively [17]. A hot-rod phantom of diameter 40 mm and with rods of diameter $1.5 - 3.0$ mm was scanned in the microPET scanner. The phantom was filled with between $1.0 - 1.5$ mCi of FDG and scanned for 2 minutes in the centre of the scanner, and for 5 minutes at a radial distance of 54 mm. The data were reconstructed with ISRA using the Redistribution technique, and compared to reconstructions with OSEM using the standard Gaussian convolution technique, as well as a commercial maximum a-posteriori (MAP) OSEM reconstruction algorithm by Siemens. The ISRA and OSEM reconstructions were performed using 20 iterations and 9 subsets, and the MAP-OSEM reconstruction used 2 OSEM iterations and 9 subsets followed by 18 MAP iterations, with a target resolution of 0.5 mm and enforcing uniform resolution. The MAP-OSEM algorithm models the resolution using PSF tables based on point source measurements for this particular scanner. The pixel size of all reconstructions was $[0.4745, 0.4745, 0.796]$ mm.

IV. Results

The reconstructions of the centred phantom are shown in figure 2 with two profiles through the reconstructions shown in figure 3. The ground truth image was created and scaled to have the same total activity as the Siemens reconstruction, and the total activities in all reconstructions are equal to within

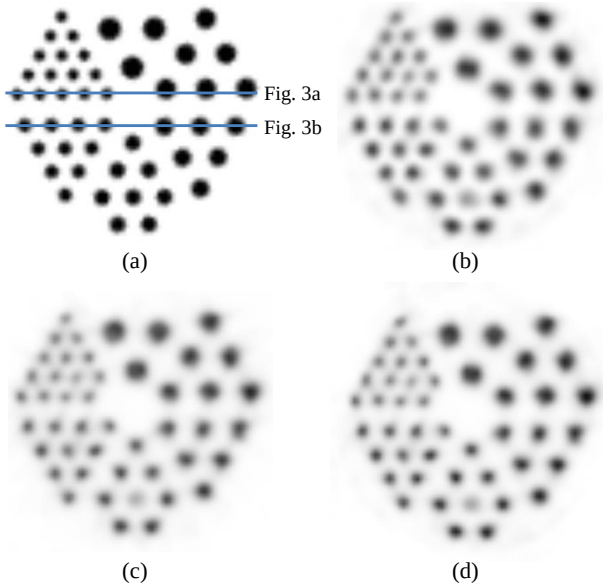

Fig. 2. Reconstructions of the centred phantom: (a) the ground truth; (b) reconstruction using the standard Siemens software (a MAP-OSEM algorithm); (c) using ISRA and the Redistribution technique; (d) using OSEM and the standard Gaussian convolution model. All images are shown to the same scale. Note that the smallest rod closest to the centre had an air pocket and did not contain any activity during the scan.

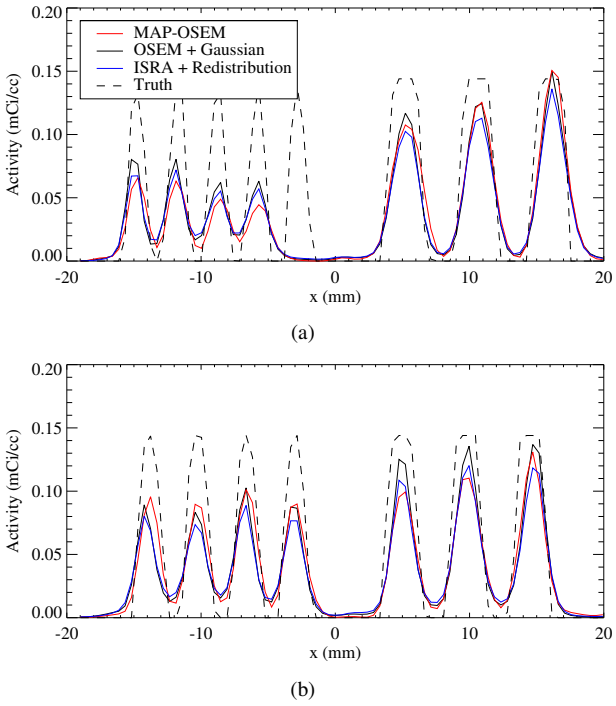

Fig. 3. Profiles through the reconstructions shown in figure 2.

4%. All three algorithms have produced very similar reconstructions with regards to resolution recovery, as expected for a phantom near the FOV centre.

The reconstructions of the off-centre phantom are shown in figures 4 and two profiles in figures 5. Due to limitations in the commercial software, it was not possible to reconstruct this data using the Siemens MAP-OSEM algorithm since

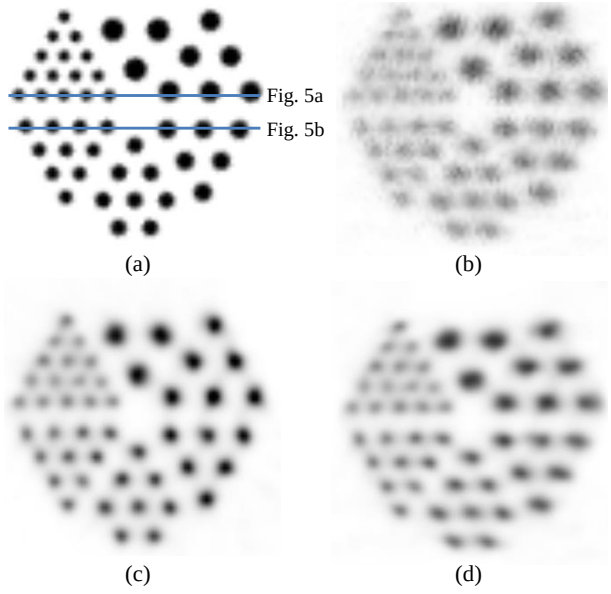

Fig. 4. Reconstructions of the off-centre phantom (positioned 54 mm to the right of the FOV centre): (a) the ground truth; (b) reconstruction using OSEM without any resolution modelling; (c) using ISRA and the Redistribution technique; (d) using OSEM and the standard Gaussian convolution model. All images are shown to the same scale. Note that the circular shape of the rods has been preserved in (c) but have been distorted away from the FOV centre (i.e. to the right) in (d).

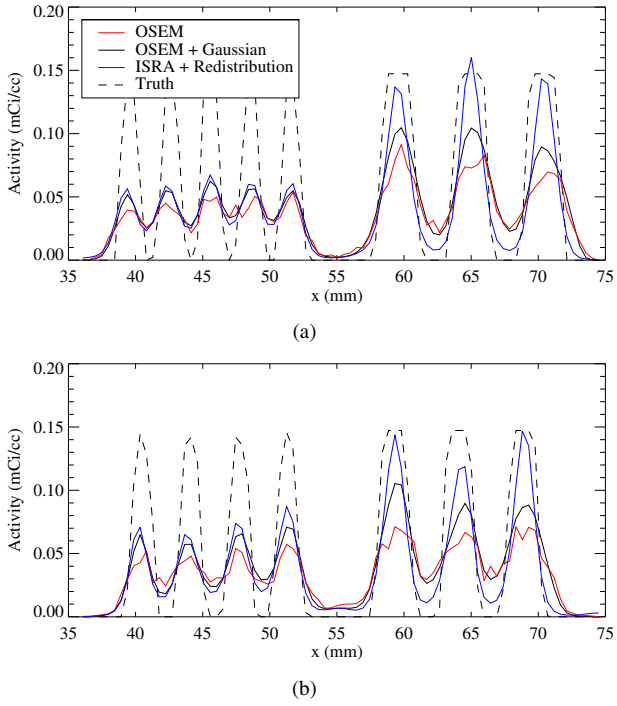

Fig. 5. Profiles through the reconstructions shown in figure 4.

the phantom was outside the reconstructable volume. For comparison's sake, the data was reconstructed using OSEM without any resolution modelling. The total activity of the reconstructions are equal to within 0.01%, and the ISRA reconstruction was used to scale the ground truth image. The Redistribution technique has produced a reconstruction with a superior resolution recovery to the Gaussian convolution model, as can be seen in figure 5. It has also preserved the circular shape of the rods while the Gaussian model has distorted them away from the FOV centre (i.e. to the right). Both models have produced better resolution recovery than the reconstruction without any resolution modelling, as expected.

The projectors used for these reconstructions were ray-tracing projectors and since the pixel size was smaller than the detector bin size, one can see the associated artefacts in figure 4(b). The distance-driven projector is known to solve this issue, however it is not easy to implement for list-mode data. It is interesting to note that both resolution modelling techniques removed these artefacts.

V. Conclusion

The Redistribution technique, a resolution modelling technique which models the system response on-the-fly during iterative reconstruction, has been presented. The system response is described analytically using PDFs which are sampled to redistribute the endpoints of the LORs used during the reconstruction. By adjusting the endpoints of the LORs in this way, a system matrix is estimated which varies radially, axially and transaxially.

It was found that the formulation of the MLEM algorithm is not well-suited to use the Redistribution technique, and so the ISRA algorithm was used as an alternative. A comparison of phantom reconstructions using standard Siemens software (a MAP-OSEM algorithm), the OSEM algorithm with and without resolution modelling using a stationary Gaussian convolution, and the ISRA algorithm with the Redistribution technique demonstrated that all the algorithms produce very similar reconstructions for phantoms near the centre of the scanner FOV, as expected, while the latter produces reconstructions with superior resolution recovery for off-centre phantoms. The Redistribution technique accurately preserves the shape of the imaged object and does not distort the reconstructions away from the centre, as the Gaussian convolution technique does.

A reconstruction using the Redistribution technique takes just under 35% more time than the standard Gaussian approach, and further optimisation is being investigated. This approach is being extended to be used with motion correction, where the movement of the subject could make the spatially variant nature of the resolution more significant.

References

[1] S. E. Derenzo, "Mathematical Removal of Positron Range Blurring in High Resolution Tomography," *IEEE Trans. Nucl. Sci.*, vol. 33, no. 1, pp. 565–569, 1986.

[2] A. Reader, P. Julyan, H. Williams, D. Hastings, and J. Zweit, "EM Algorithm System Modeling by Image-Space Techniques for PET Reconstruction," *IEEE Trans. Nucl. Sci.*, vol. 50, no. 5, pp. 1392–1397, Oct. 2003.

[3] M. G. Bickell, L. Zhou, and J. Nuyts, "Spatially Variant Resolution Modelling for Iterative List-Mode PET Reconstruction," *IEEE Nucl. Sci. Symp. Conf. Rec.*, 2013.

[4] S. Moehrs, M. Defrise, N. Belcari, A. D. Guerra, A. Bartoli, S. Fabbri, and G. Zanetti, "Multi-ray-based system matrix generation for 3D PET reconstruction," *Phys. Med. Biol.*, vol. 53, no. 23, pp. 6925–45, Dec. 2008.

[5] Y. Chen and S. J. Glick, "Determination of the System Matrix Used in List-Mode EM Reconstruction of PET," *IEEE Nucl. Sci. Symp. Conf. Rec.*, pp. 3855–3858, 2007.

[6] M. G. Bickell, A. Buffler, and I. Govender, "A fully 4D mesh parameterisation PET image reconstruction algorithm for list-mode data," *IEEE Nucl. Sci. Symp. Conf. Rec.*, pp. 2620–2624, Oct. 2011.

[7] E. Gonzalez, J.-y. Cui, and G. Pratx, "Point spread function for PET detectors based on the probability density function of the line segment," *IEEE Nucl. Sci. Symp. Conf. Rec.*, pp. 4386–4389, 2011.

[8] X. Jin, C. Chan, T. Mulnix, V. Panin, M. E. Casey, C. Liu, and R. E. Carson, "List-mode reconstruction for the Biograph mCT with physics modeling and event-by-event motion correction," *Phys. Med. Biol.*, vol. 58, no. 16, pp. 5567–5591, Jul. 2013.

[9] J. E. Gillam, P. Solevi, J. F. Oliver, and M. Rafecas, "Simulated one-pass list-mode: an approach to on-the-fly system matrix calculation," *Phys. Med. Biol.*, vol. 58, no. 7, pp. 2377–94, Apr. 2013.

[10] A. Autret, J. Bert, O. Strauss, and D. Visvikis, "Fully 3D PET List-Mode reconstruction including an accurate detector modeling on GPU architecture," *Fully 3D 2013*, pp. 229 –232, 2013.

[11] M. Daube-Witherspoon and G. Muehllehner, "An iterative image space reconstruction algorithm suitable for volume ECT," *IEEE Trans. Med. Imaging*, vol. 5, no. 2, pp. 61–66, 1986.

[12] L. Parra and H. H. Barrett, "List-mode likelihood: EM algorithm and image quality estimation demonstrated on 2-D PET," *IEEE Trans. Med. Imaging*, vol. 17, no. 2, pp. 228–35, Apr. 1998.

[13] A. J. Reader, K. Erlandsson, M. A. Flower, and R. J. Ott, "Fast accurate iterative reconstruction for low-statistics positron volume imaging," *Phys. Med. Biol.*, vol. 43, no. 4, pp. 835–46, Apr. 1998.

[14] H. M. Hudson and R. S. Larkin, "Accelerated image reconstruction using ordered subsets of projection data," *IEEE Trans. Med. Imaging*, vol. 13, no. 4, pp. 601–609, 1994.

[15] D. M. Titterington, "On the Iterative Image Space Reconstruction Algorithm for ECT." *IEEE Trans. Med. Imaging*, vol. 6, no. 1, pp. 52–6, Jan. 1987.

[16] A. Reader, E. Letourneau, and J. Verhaeghe, "Generalization of the image space reconstruction algorithm," *IEEE Nucl. Sci. Symp. Conf. Rec.*, no. 6, pp. 4233–4238, 2011.

[17] Y.-C. Tai, A. Ruangma, D. Rowland, S. Siegel, D. F. Newport, P. L. Chow, and R. Laforest, "Performance evaluation of the microPET Focus: a third-generation microPET scanner dedicated to animal imaging," *J. Nucl. Med.*, vol. 46, no. 3, pp. 455–63, Mar. 2005.